Supporting Information

Polacheck et al. 10.1073/pnas.1103581108

SI Materials and Methods

Device Fabrication. Microfluidic devices were fabricated using soft lithography in a process that has been described previously (1). Polydimethylsiloxane (PDMS) was mixed at 10:1 base:curing agent, poured over a silicon master, and incubated overnight at 80 °C. The PDMS was cut from the silicon master, trimmed, and autoclaved in water. The devices were then dry autoclaved and dried overnight in an oven at 80 °C. The sterile PDMS devices were then surface activated by plasma treatment for 2 min (Harrick Plasma), coated with poly-D-lysine (PDL; Sigma-Aldrich), incubated overnight at 37 °C, washed with sterile water, and dried overnight at 80 °C. The gel–cell solution (*Materials and Methods*) was added to the devices by hand using a micropipette, and devices were sealed with a coverslip. The seeded devices were placed in an incubator at 37 °C for 30 min to allow the collagen gel to polymerize before adding media. Reservoirs for establishing pressure head were made from modified Nalgene (Thermo Fisher Scientific) bottles with Tygon (Compagnie de Saint-Gobain) tubing to connect the reservoirs to the device.

Finite Element Model (FEM) for Determination of Streamlines. A FEM was developed in Comsol Multiphysics (COMSOL), using an imported Auto-CAD file (Autodesk) of the device geometry. The model was implemented to determine the fluid velocity vector field by solving Brinkman's equation for flow through a porous medium (2),

$$\mu\nabla^2 \underline{v} - \frac{\mu}{\kappa}\underline{v} - \nabla P = 0, \qquad \text{[S1]}$$

where μ is the fluid viscosity, K is the permeability, and P is the pressure drop. The model solved Brinkman's equation for the full 3D geometry of the device in steady state. The permeability was determined experimentally (*Results*) and assumed to be constant throughout the region of the device with collagen gel. The pressure drop was determined for each experiment by measuring the hydrostatic pressure difference between the upstream and downstream reservoirs. No-slip boundary conditions were applied at the PDMS walls.

Alignment Quantification. For cell alignment quantification, images at given time points were segmented using a previously described Matlab (The Math Works) script (3). An in-house Matlab script fit an ellipse to each segmented cell, and the location of the centroid of each ellipse was passed to COMSOL to determine the flow velocity vector local to each cell's centroid. A Matlab script was used to convert the segmented cell field to a vector field by generating vectors from the centroid along the major axis of each ellipse. The local angle of alignment was determined by computing the dot product between the local streamline vector from COMSOL and the local cell vector. Subsequent vector analysis and quantification were performed using an in-house Matlab script.

Migration Quantification. Cells were tracked in time-lapse image sequences using the manual tracking plug-in for ImageJ (4) (http://rsb.info.nih.gov/ij). An in-house Matlab script determined migration position and velocity vectors from the ImageJ output. The origin of the migration vectors was passed to COMSOL to determine the local fluid velocity vector. Further vector analysis was performed in Matlab using an in-house script. Migration data for each cell in one device were averaged over the whole cell population (>15 cells for each device), and the average migration data for each cell population were averaged over multiple devices (three or more devices for each condition). Statistics were tabulated using a one-way analysis of variance (ANOVA).

Flow Verification. To quantify the flow field, 200-nm fluorescent microspheres were added to the cell media in the upstream reservoir. Microspheres were imaged using fluorescent time-lapse images. Images were binarized using ImageJ, and an automated tracking algorithm in IMARIS (Bitplane) was used to track the beads in the binarized time-lapse images. An in-house Matlab script determined velocity vectors for each bead, using the IMARIS output. The origin of each bead was passed to COMSOL to determine the local velocity vector. Subsequent vector analysis, including computation of angle between experimental and predicted velocity vectors, was performed in Matlab.

Model for Transcellular Autocrine Morphogen Gradient for a Multicell Population. To determine the effects of cell concentration on autocrine gradients in an interstitial flow field, a coupled mass and momentum transport FEM was developed in COMSOL. The geometry used to model cells in a porous matrix consisted of five cells, with each cell modeled as a sphere with radius of 10 μm, and the distance between each cell center was 20 μm (Fig. S3). Brinkman's equation (Eq. **S1**) (2) was solved for the given geometry. No-slip boundary conditions were applied at the cell walls, and zero normal velocity was imposed between cells at the lateral boundary. The inlet velocity was fixed at 3.0 μm/s to match experimental conditions, and the permeability was determined experimentally (*Results*).

The velocity field determined from Brinkman's equation was then used to solve the diffusion equation

$$\frac{dC}{dt} + \nabla\cdot N - R = 0$$
$$N = -D\nabla C + v\cdot C, \qquad \text{[S2]}$$

where C is the concentration of morphogen, N is the molar flux, v is the velocity determined from Brinkman's equation, D is the diffusivity of the morphogen in the given medium, and R accounts for addition or consumption of the morphogen due to reaction. The diffusivity for CCL21 in water was used (5), and a variety of reaction rates were considered. Constant flux boundary conditions were imposed at cell surfaces, no flux boundary conditions were imposed at the lateral symmetric boundary between cells, a zero concentration boundary condition was imposed at the inlet, and a zero diffusive flux boundary condition was imposed at the outlet. Steady state was assumed as we intended to model the concentration field at long times. The resulting morphogen concentration fields were exported to Matlab for further analysis of transcellular concentration gradients. We varied the reaction rate from 0 to $-0.2\ s^{-1} \times C$ (5) and observed that increased cell density decreased the relative magnitude of chemokine gradients for these reaction rates.

Force on Cells Due to Fluid Flow Through Porous Media. The net pressure force on a cell exposed to flow in a porous medium can be determined from Darcy's law:

$$\nabla P : \frac{\Delta P}{R} : \frac{\mu}{\kappa} v. \qquad \text{[S3]}$$

P is the pressure, R is the characteristic length (radius of the cell), μ is viscosity, κ is permeability, and v is the fluid velocity.

As demonstrated by Tam, $\kappa^{-1/2}$ is the characteristic length (the "screening length") over which velocity goes to zero at the surface of the cell (6). Therefore, the shear stress at the cell surface can be estimated by the expression

$$\tau : \frac{\mu}{\sqrt{\kappa}} v. \qquad [S4]$$

By taking the ratio of the force due to the Darcy pressure drop to the force due to shear stress, we can compare the relative magnitudes of each force:

$$\frac{F_{pm}}{F_s} : \frac{P \cdot R^2}{\tau \cdot R^2} : \left(\frac{\mu R}{\kappa} v\right)\left(\frac{\mu}{\sqrt{\kappa}} v\right)^{-1} : \frac{R}{\sqrt{\kappa}}. \qquad [S5]$$

The results of this analysis are consistent with the formulation for drag on a sphere in a Brinkman medium determined by Ganapathy (7).

To verify the scaling analysis above, an FEM was developed using Comsol Multiphysics (COMSOL). The model was implemented to determine the fluid pressure field by solving Brinkman's equation for flow through a porous medium (Eq. **S1**). The model solved Brinkman's equation for a rectangular domain with an embedded cylinder of 10-μm radius and assumed a constant permeability of 1×10^{-13} m^2, determined from the bead tracking data (*Results*). Informed by the bead tracking data, the inlet velocity was 3 μm/s, and no-slip boundary conditions were applied at the cylinder walls. The fluid pressure was determined at the walls of the cylinder to approximate the pressure of a cell in a porous ECM. The results were consistent with the scaling analysis in Eq. **S3**.

Data

Cell alignment. When exposed to interstitial flow, cells aligned parallel to flow streamlines (Fig. S1*A*). Cell alignment was quantified by measuring the angle between the major axis of an ellipse fit to each cell and the local flow velocity vector from an FEM of the flow field. At longer times, after 48 h, cells extended protrusions and subsequently formed multicell strings in parallel with the flow streamlines; after 40 h, cells exposed to flow velocities of 3.0 μm/s aligned with the streamlines of the flow field with 86 ± 7% of cells aligned within 45° of the local streamline. Cells not exposed to flow remained randomly oriented with only 55 ± 2% of cells within 45° of the local streamline (Fig. S1). The time required for alignment demonstrates that cells were actively responding to a stimulus from the flow and not simply being stretched by the pressure drop across the gel. Cell alignment with the flow streamlines is consistent with the work of Levesque and Nerem, who demonstrated that endothelial cells align in response to 2D shear flow (7).

Cell migration. Interstitial flow did not have a significant effect on cell migration velocity, defined as total migration distance over a given time (Fig. S2*A*). Directionality, also referred to as directional persistence, is a measure of how straight a cell migrates and has been used previously to demonstrate the effect of chemokines on cell migration behavior (8). Directionality is defined as the net migration distance normalized by the total migration distance, and cells exposed to interstitial flow migrated with increased directionality (Fig. S2*B*). Cell motility, another metric used to quantify cell response to chemokines, is defined as the percentage of cells migrating a distance greater than one cell diameter and was unaffected by flow (Fig. S2*C*). In other words, interstitial flow does not affect the percentage of the cell population that migrates or the speed at which the cells migrate, but migrating cells exposed to interstitial flow will migrate a larger net distance in a given time.

Transcellular gradients in multicell populations. The effect of interstitial flow on autologous morphogen gradients has been previously studied in the context of autologous chemotaxis (5), but the computational model presented considers only one cell in the presence of a flow field. Our results on the effect of interstitial flow on direction of cell migration demonstrate that migration bias in a cell population is a function of cell density, and we hypothesize that the cell density dependence was the result of the interaction between morphogen fields among neighboring cells.

To test this hypothesis we developed a computational model to investigate the magnitude of transcellular gradient as a function of cell density. Transcellular chemokine gradients lead to chemotaxis and can guide the direction of cell migration (9). To quantify the transcellular gradient, we used a metric similar to the metric used by Fleury et al. to determine the transcellular gradient for single cells in interstitial flow (5) and similar to metrics used in chemotaxis assays (10). The transcellular gradient is defined as $(\Delta C/C_m) \times 100$, where ΔC is the difference in concentration between the downstream and upstream ends of the cell, and C_m is the concentration at the center of the cell. We found that as more cells are located upstream, the transcellular gradient decreased (Fig. S3). In other words, increasing the cell density introduces more cells upstream and results in a lower-magnitude transcellular autocrine gradient.

Effect of PP2 on cell migration. It has been shown that FAK activates Src kinase (11–13), which modulates traction forces important for tumor cell migration (14, 15). To examine the role of shear stress-induced FA activation on migration in the presence interstitial flow, we introduced the specific inhibitor of Src kinase PP2 (11, 16). We found that inactivation of Src kinase blocked directional migration of cells exposed to interstitial flow. For cells seeded at 25×10^4 cells/mL, the streamline migration score was not significantly different from 0 for control, 0.3 μm/s, and 3.0 μm/s applied flow (Fig. S5*A*). Furthermore, the directional migration scores at 0.3 μm/s and 3.0 μm/s applied flow did not vary significantly from control (Fig. S5*B*). Cell migration velocity was unchanged with the addition of PP2, but cell migration was randomly directed, suggesting that Src kinase is involved with directional sensing for cells exposed to interstitial flow.

These data are consistent with the CCR7-mediated autologous chemotaxis model for downstream migration because Src has been implicated in the CCR7 pathway in lymphocytes (17, 18). Because PP2 blocked upstream migration as well, Src is also apparently involved in upstream migration; furthermore, upstream migration is independent of cell density, so paracrine and autocrine signaling through chemokine receptors are unlikely stimuli for Src activation. Consequently, the PP2 data support our hypothesis that flow-induced stress gradients and directed proteolysis lead to directional bias in integrin activation, FA formation, and subsequent Src activation, stimulating migration against the flow.

1. Vickerman V, Blundo J, Chung S, Kamm RD (2008) Design, fabrication and implementation of a novel multi-parameter control microfluidic platform for three-dimensional cell culture and real-time imaging. *Lab Chip* 8:1468–1477.
2. Brinkman HC (1947) A calculation of the viscous force exerted by a flowing fluid on a dense swarm of particles. *Appl Sci Res* A1:27–34.
3. Bakal C, Aach J, Church G, Perrimon N (2007) Local signaling networks that regulate cell morphology defined by quantitative morphological signatures. *Science*, 316: 1753–1756. Available at http://rsbweb.nih.gov/ij/plugins/track/track.html. Accessed on January 8, 2009.
4. Cordelires F (2004) Manual tracking plugin for ImageJ.
5. Fleury ME, Boardman KC, Swartz MA (2006) Autologous morphogen gradients by subtle interstitial flow and matrix interactions. *Biophys J* 91:113–121.
6. Tam CKW (1969) The drag on a cloud of spherical particles in low Reynolds number flow. *J Fluid Mech* 38:537–546.

7. Levesque MJ, Nerem RM (1985) The elongation and orientation of cultured endothelial cells in response to shear stress. *J Biomech Eng* 107:341–347.
8. Ware MF, Wells A, Lauffenburger DA (1998) Epidermal growth factor alters fibroblast migration speed and directional persistence reciprocally and in a matrix-dependent manner. *J Cell Sci* 111:2423–2432.
9. Tranquillo RT, Lauffenburger DA, Zigmond SH (1988) A stochastic model for leukocyte random motility and chemotaxis based on receptor binding fluctuations. *J Cell Biol* 106:303–309.
10. Wang SJ, Saadi W, Lin F, Minh-Canh Nguyen C, Li Jeon N (2004) Differential effects of EGF gradient profiles on MDA-MB-231 breast cancer cell chemotaxis. *Exp Cell Res* 300: 180–189.
11. Thomas JW, et al. (1998) SH2- and SH3-mediated interactions between focal adhesion kinase and Src. *J Biol Chem* 273:577–583.
12. Eide BL, Turck CW, Escobedo JA (1995) Identification of Tyr-397 as the primary site of tyrosine phosphorylation and pp60src association in the focal adhesion kinase, pp125FAK. *Mol Cell Biol* 15:2819–2827.
13. Schaller MD, et al. (1994) Autophosphorylation of the focal adhesion kinase, pp125FAK, directs SH2-dependent binding of pp60src. *Mol Cell Biol* 14:1680–1688.
14. Fincham VJ, Frame MC (1998) The catalytic activity of Src is dispensable for translocation to focal adhesions but controls the turnover of these structures during cell motility. *EMBO J* 17:81–92.
15. Sieg DJ, et al. (1998) Pyk2 and Src-family protein-tyrosine kinases compensate for the loss of FAK in fibronectin-stimulated signaling events but Pyk2 does not fully function to enhance FAK- cell migration. *EMBO J* 17:5933–5947.
16. Jalali S, et al. (1998) Shear stress activates p60src-Ras-MAPK signaling pathways in vascular endothelial cells. *Arterioscler Thromb Vasc Biol* 18:227–234.
17. Bardi G, Niggli V, Loetscher P (2003) Rho kinase is required for CCR7-mediated polarization and chemotaxis of T lymphocytes. *FEBS Lett* 542:79–83.
18. Riol-Blanco L, et al. (2005) The chemokine receptor CCR7 activates in dendritic cells two signaling modules that independently regulate chemotaxis and migratory speed. *J Immunol* 174:4070–4080.

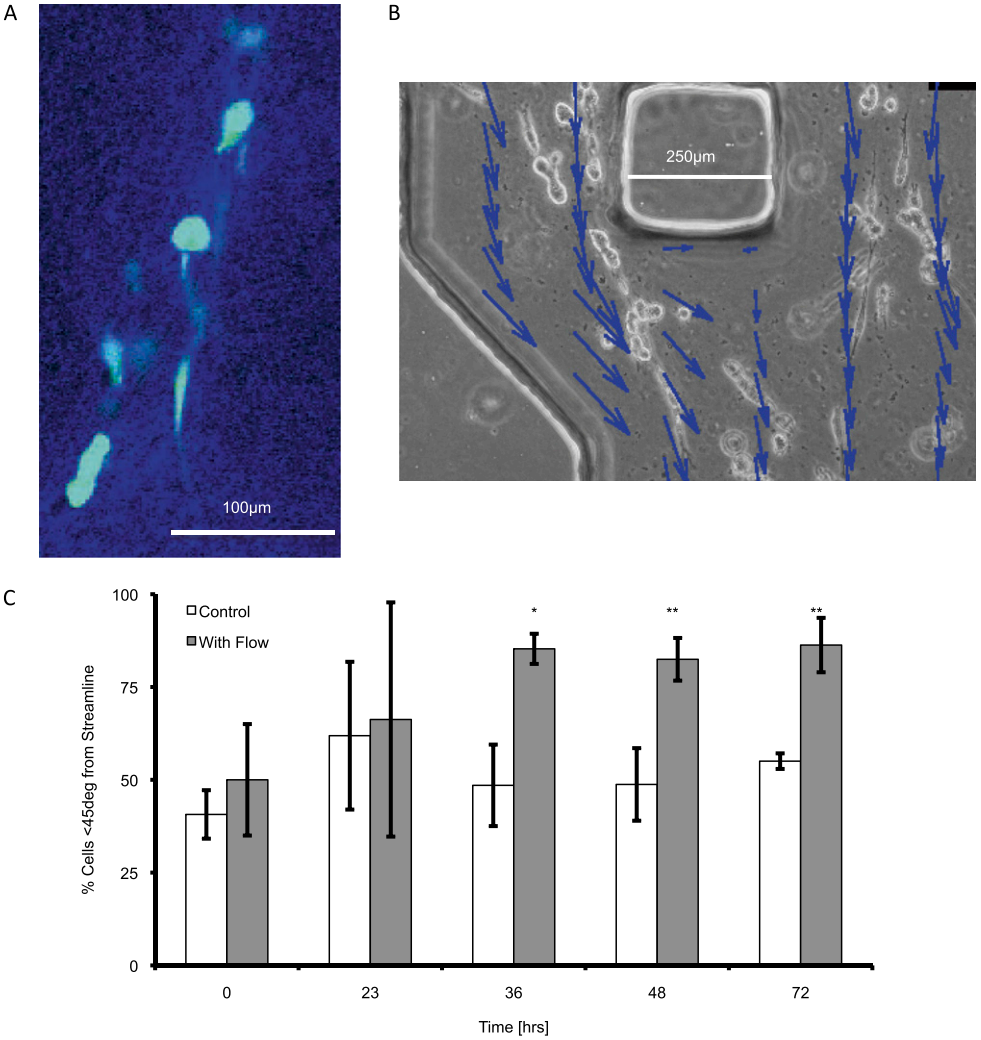

Fig. S1. Interstitial flow induces cell alignment to flow streamlines. (*A*) Confocal reflectance image showing cell and collagen fiber alignment to flow (flow is top to bottom) taken 48 h after applying 3 μm/s flow. (*B*) Streamline vectors from FEM of flow in the device superimposed on a phase contrast image of cells exposed to flow. (*C*) Angle of alignment was quantified by fitting an ellipse to each cell and plotting a vector from the centroid along the major axis of the ellipse. The dot product between the cell alignment vector and local streamline vector from an FEM was computed. Over time, a greater percentage of the cell population aligned to the streamlines (*$P < 0.05$; **$P < 0.01$).

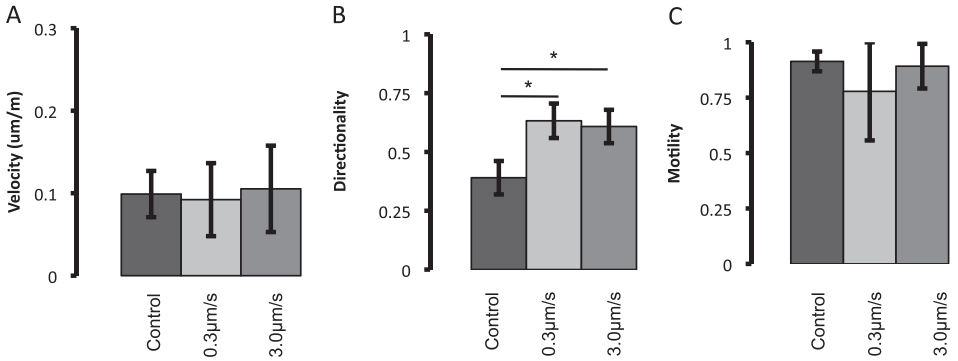

Fig. S2. (*A*–*C*) Interstital flow affects cell migration. Although flow had no affect on migration velocity or cell population motility, it significantly increased the directionality of migrating cells (*$P < 0.05$).

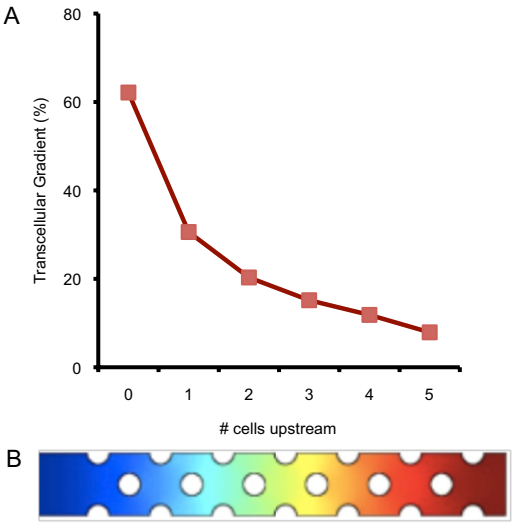

Fig. S3. Transcellular morphogen gradients are a function of cell density. (*A*) Transcellular gradients, defined as $(\Delta C/C_m) \times 100$, can lead to chemotaxis toward increasing concentration of chemokine. Increasing the concentration of cells increases the number of upstream cells, and these cells contribute to a decreased transcellular autocrine chemokine gradient. In these data, $R = 0$, but similar trends are observed for physiologic reaction rates (5). (*B*) Absolute concentration of chemokine is a function of cell density. Color denotes normalized chemokine concentration (C/C_{Max}), blue indicates $C/C_{Max} = 0$, and red indicates maximum concentration $C/C_{Max} = 1$. White circles indicate cells, and cells are aligned with the *x* axis of *A* to demonstrate the relationship between concentration field and concentration gradient.

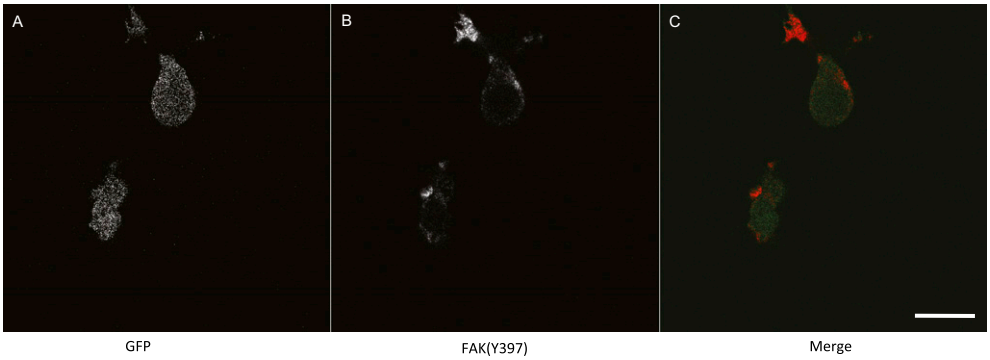

Fig. S4. FAK phosphorylation is localized to the cell membrane. (*A*–*C*) GFP (*A*), FAK(Y397) (*B*), and overlay of GFP in green and FAK(Y397) in red (*C*) for a single z-slice of cells exposed to 3.0 μm/s flow. Flow is from top to bottom of image. (Scale bar, 10 μm.)

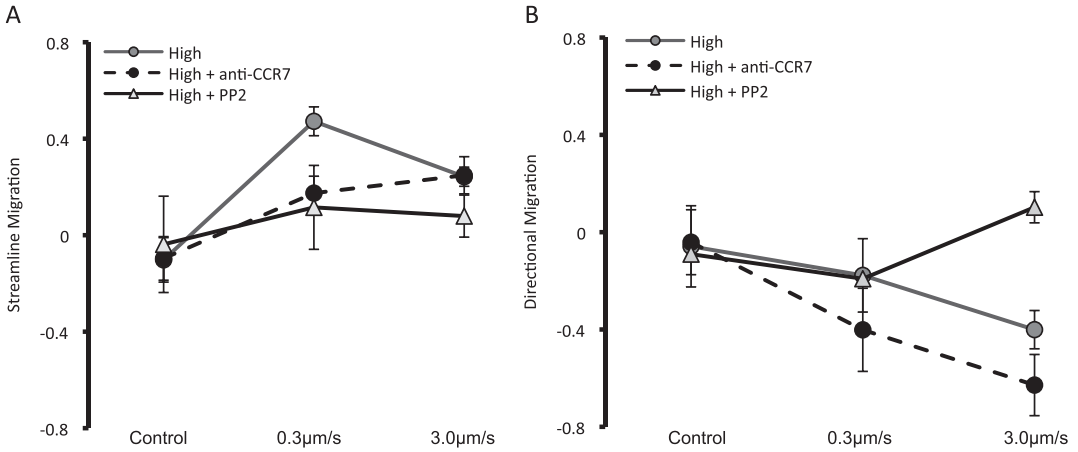

Fig. S5. Addition of specific inhibitor of Src kinase. PP2 blocked directional migration of cells exposed to interstitial flow. (*A*) In devices at both flow rates, streamline migration scores were not different from 0. (*B*) The directional migration score did not vary from control for both flow rates with the addition of PP2. (Mean ± SD was computed by averaging the score for each cell in one device ($n > 15$) and averaging the score for three devices at each condition.)